An Acad Bras Cienc (2020) 92(3): e20181323 DOI 10.1590/0001-3765202020181323
Anais da Academia Brasileira de Ciências | *Annals of the Brazilian Academy of Sciences*
Printed ISSN 0001-3765 I Online ISSN 1678-2690
www.scielo.br/aabc | www.fb.com/aabcjournal

CHEMICAL SCIENCES

Partial inclusion of bis(1,10-phenanthroline) silver(I) salicylate in β-cyclodextrin: Spectroscopic characterization, *in vitro* and *in silico* antimicrobial evaluation

EDWIN BRIÑEZ-ORTEGA, VERA L. DE ALMEIDA, JULIO C. D. LOPES & ANA E. BURGOS

Abstract: Silver complexes containing 1,10-phenanthroline as a coordinated ligand have been of great interest due to their antibacterial and antifungal pharmacological properties. In this paper, we describe the synthesis of a new partial inclusion complex of bis(1,10-phenanthroline)silver(I) salicylate in β-cyclodextrin (β-CD) which was synthesized with a good yield. The compounds were characterized by FTIR, ^{1}H, ^{13}C NMR including ^{1}H–^{1}H COSY, TGA/DSC, elemental analysis (CHN), and X-ray powder diffraction. The results suggest the presence of non-covalent interactions such as hydrogen bonds, van der Waals forces, and hydrophobic interactions in the formation of the partial inclusion compound between β-CD and bis(1,10-phenanthroline)silver(I) salicylate $[Ag(phen)_2]$salH. Additionally, an *in silico* prediction of 1,10-phenanthroline biological activities was carried out and the acquired data suggests several potential targets associated with the antimicrobial activity of this compound and its silver complex. Most predicted targets are related to antimicrobial virulence and resistance that are a serious threat to global public health. The inclusion compound showed a higher inhibiting growth of *Candida albicans* than the free complex $[Ag(phen)_2]$salH indicating that the formation of the inclusion complex with β-CD increases the bioavailability of the antimicrobial active species $[Ag(phen)_2]^+$ of the new silver(I) compound.

Key words: Bis(1,10-phenanthroline)silver(I), β-cyclodextrin, *in silico* prediction, SVM modeling, antimicrobial.

INTRODUCTION

Silver complexes containing 1,10-phenanthroline as a coordinated ligand have been of great interest due to their antibacterial and antifungal pharmacological properties and anticancer activity, for example in breast cancer; furthermore, there are no reported side effects such as toxicity or clinical problems (Deegan et al. 2007, Shahabadi et al. 2014, Viganor et al. 2017). The use of salicylate bis(1,10-phenanthroline)silver(I) $[Ag(phen)_2]$salH stands out as an antibacterial and cytotoxic agent in breast, ovarian and lung cancers (Thornton et al. 2016). These properties are attributed to the presence of silver(I) ions and ligands such as the salicylate and 1,10-phenanthroline which have proven biological activities.

It has been suggested that the potentially active species of the silver compounds is the $[Ag(phen)_2]^+$ ion, that is interacting through the intercalation among DNA chains resulting in the cell's death (Moyano et al. 2005, Deegan et al. 2007, Viganor et al. 2017). The main disadvantage of coordinating the compound $[Ag(phen)_2]$salH is its low solubility in water due to its

hydrophobic character caused by the presence of 1,10-phenanthroline in the molecule. This fact makes the distribution of silver(I) complex in the cellular medium difficult and prevents its effective transport to the inside of the cell. For this reason, processes that improve the biological interaction mechanisms of silver(I) compounds in the cellular system have been investigated (Coyle et al. 2003, Moyano et al. 2012, Shahabadi et al. 2014).

Cyclodextrins (CDs) are cyclic oligomers constituted of glucopyranose units bonded through α (1→4) glucosidic linkages. The most common are α, β and ɣ-CD formed by six, seven and eight glucose units, respectively. The structure of these compounds has the shape of a truncated cone. The presence of secondary hydroxyl groups form the larger base and the primary hydroxyl groups form the smaller base of the truncated cone, providing a hydrophilic exterior and a hydrophobic cavity (Liu et al. 2015).

The hydrophobic cavity of CDs can host a variety of organic and inorganic molecules forming host/guest complexes with noncovalent interactions that involve van der Waals forces, hydrophobic interactions and hydrogen bonds. These interactions modify the physical and chemical properties of the host compound inserted in CDs (Duchêne & Bochot 2016, Lucio et al. 2017). In this context, CDs are used for improving the biological properties of chemotherapeutic agents, for the release of drugs, for increasing the compound solubility in water, for improving the chemical stability and bioavailability of pharmacological compounds, and for toxicity reduction (Burgos & Sinisterra 2010, Lucio et al. 2017).

The aim of the present work was to prepare and characterize the structure of the partial inclusion complex formed by partial inclusion of bis(1,10-phenanthroline)silver(I) salicylate [Ag(phen)$_2$]salH in β-CD. This inclusion was chosen as a strategy to increase the solubility in water of the complex [Ag(phen)$_2$]salH improving its pharmacokinetic properties and, consequently, its biological activity. The structure of the complex [Ag(phen)$_2$]salH-β-CD and the chemical interactions between [Ag(phen)$_2$]salH and β-CD were studied by means of the Fourier transform infrared (FTIR), nuclear magnetic resonance of hydrogen and carbon (^{1}H, and ^{13}C NMR, including ^{1}H-^{1}H COSY) spectroscopies, powder X-ray diffractometry, elemental analysis (CHN) and also by simultaneous thermogravimetry differential scanning calorimetry (TGA/DSC) analysis. Previously, the property of [Ag(phen)$_2$]salH to inhibit the *in vitro* growth of pathogenical bacterial strains *Micrococcus luteos* and *Escherichia coli* was observed by Moyano et al. (2012). Thus, the antimicrobial activity of free compounds [Ag(phen)$_2$]salH, β-CD and the complex [Ag(phen)$_2$]salH-β-CD were evaluated using the *in vitro* radial diffusion method. In addition, to support the *in vitro* assays data, some insights were gathered about potential biological targets with an *in silico* prediction of 1,10-phenanthroline biological activities.

MATERIALS AND METHODS

General experimental procedures

Chemicals, cell culture reagents and media were purchased from commercial sources and were used without further purification. β-cyclodextrin of high purity were purchased from Sigma-Aldrich and were used as received. Distilled water to prepare the solutions was used.

Melting points (mp) (uncorrected) were determined using a Mel-Temp II melting point apparatus (Laboratoy Devices Inc.). The FTIR spectra of samples, at ~1% KBr solution, were recorded on a Thermo Scientific Nicolet iS10

FT-IR Spectrometer with 16 scans at 4 cm^{-1} resolution. The ^1H and ^{13}C NMR spectra were recorded at 400.129 and 100.613 MHz, respectively, as well as correlation spectroscopy ^1H-^1H (COSY) was performed on a Brüker DRX400 AVANCE spectrometer, using DMSO-d_6 as a solvent, with direct or inverse probes and a field gradient. The chemical shifts were registered in ppm (δ) using TMS as the internal standard (δ_H = δc = 0). The coupling constants (J) were registered in Hertz (Hz). The X-ray diffraction profiles were collected at room temperature using a Panalytical X'Pert PRO (Cu Kα radiation, λ = 1.54056 Å) instrument with 2θ, from 5° 2θ to 70° 2θ, step size of 0.01° (2θ) and step time of 10 s. The sample holder was subjected to spinning at 30 cycles per minute to minimize rugosity effects and to reduce any eventual preferred orientation. The lattice parameters were extracted and fitted by Rietveld fitting analysis. TGA/DSC thermal decomposition analysis were performed on a Rheometrics STA 500 equipment (Scientific Reometrics Inc.) under argon and heating ramp of 10 °C/min. Elemental analysis was performed on a CHN-660, carbon-hydrogen-nitrogen determinator, Leco Corporation ST. Joseph, MI USA.

Preparation and characterization of the inclusion complex

The [Ag(phen)$_2$]salH was synthesized following the reaction method established by Moyano et al. (2012), obtaining a similar percentage yield, and its purity was checked by thin layer chromatography. The obtained results are in accordance with those calculated, and suggest obtaining a minimum formula compound [Ag(phen)$_2$]salH, yield of 79%, and the melting point: 230 ± 2 °C. The [Ag(phen)$_2$]salH [26.0 mg (0.044 mmol)] was dissolved in water (10 mL) and 50.0 mg (0.044 mmol) of β-CD was added, in molar ratio 1:1 between host and guest molecules. The reaction mixture was kept under reflux at 40-50 °C, for 48 hours. After this time, the reaction mixture was frozen at -70 °C and then lyophilized. By this process, the solid inclusion complex (SIC) was obtained as a yellowish solid material, which was soluble in water, ethanol, dimethylsulfoxide, acetaldehyde and 2-propanol, the solubility tests were carried out at room temperature and at 60 ° C and suffered decomposition at 242 °C. For physicochemical comparison purposes, a solid solution (SS) of [Ag(phen)$_2$]salH and β-CD at 1:1 molar ratio was prepared by mechanical stirring and then kept under vacuum in a dissecator, until the moment of its physicochemical analysis.

The SIC [Ag(phen)$_2$]salH-β-CD and the 1:1 SS were characterized by FTIR, ^1H and ^{13}C NMR, including ^1H-^1H COSY, and also by powder X-ray diffracttometry and elemental analyses.

Microbial growth inhibition evaluation

The antibacterial and antifungal assays of aqueous solution (500 μM) of SIC, [Ag(phen)$_2$] salH and β-CD were performed following the Kirby-Bauer disk diffusion method suggested by the Clinical and Laboratory Standards Institute (CLSI 2003). For the antibacterial tests, four disks respectively moistened with each sample of aqueous solution were used. The Gram-positive bacteria *Staphylococcus aureus* (ATCC 29213) and the Gram-negative *Pseudomonas aeruginosa* (ATCC 27853) were used in the assays by adopting a specific agar medium for each species. The antifungal property of the above samples was evaluated using *Candida albicans* (ATCC 10231). For the antifungal and antibacterial assays, disks containing 500 μM of each sample added in aqueous solution were used. Trypticase soy broth (TSB) (Difco) was used as *C. albicans* culture medium. In parallel, four disks respectively moistened with the aqueous solution (500 μM) of clotrimazol® (positive control), salicylic acid, silver nitrate, and 1,10-phenanthroline were

used as a blank. All assays were performed in triplicate and under similar conditions.

In silico prediction of 1,10-phenanthroline biological activities

The method selected to perform the prediction of the biological activity, 3D pharmacophore fingerprints, is based on the structure of the active and inactive compounds ("ligand-based approach"). Regardless of the fact that is possible to include descriptors for metallic ions, the method strongly depends on the datasets available. None of the datasets used in this paper has silver complexes thus it would not be possible to make predictions for the silver complex of the compound. In addition, the ligand bis(1,10-phenanthroline) showed to be active as expected. We think it is important to evaluate other activities of the ligand, and related then to the possible mechanism of action.

To perform the prediction of antifungal and antibacterial activities of 1,10-phenanthroline, we searched in PubChem Bioassay database (Wang et al. 2017) for all published bioassays related to *C. albicans*, *P. aeruginosa* and *S. aureus*. A total of 47 datasets that adhered to the following characteristics were selected: at least 15 active and inactive compounds and less than 30 thousand compounds in total. Two additional datasets were built by grouping several smaller datasets, totalling 49 datasets that were modeled and validated as described below.

From the bioassay data file available for each unique assay identifier (AID) in the PubChem Bioassay database, we preserved only compounds classified as active or inactive, according to PUBCHEM_ACTIVITY_OUTCOME field. The structures of all compounds were downloaded from the PubChem Compound database using the 3D option with up to ten conformations for each and converted into a unique modal of 3-point pharmacophore fingerprints (Shemetulskis et al. 1996). The full description of how the fingerprints were generated may be found in (Rocha et al. 2018).

The multi-conformation (modal) pharmacophore fingerprint of active and inactive compounds were used to build machine learning models using a support vector machine (SVM) approach with the in-house software ExCVBA (Santos et al. 2015). Support vector machine (SVM) is a supervised learning method that recognizes patterns in the descriptor space, generating a model where the instances in each category are divided by a hyperplane. When a new set of data is submitted to the SVM model it predicts to which group it belongs.

For each PubChem Bioassay data set two subsets are created through stratified random partition to produced 30 independent models. The first subset, composed of 70% is the training set and the second being composed of 30% is the validation set. The average scores of each compound in the validation set was used do assess the modeling performance with the area under the Receiver Operating Characteristic curve (AUC), as well for activity prediction of new compounds, as described below. The SVM software used to built the models were LibSVM (Chang & Lin 2011) software and linear kernel option with a 5-fold cross-validation (CV) using the Power Metric (Lopes et al. 2017, De Winter & Lopes 2018) at TPR+FPR=0.5 as the optimization objective metric to assure early recovery of active compounds.

In the prediction phase the modal multi-conformational pharmacophore fingerprints of the new compounds were submitted to all 30 SVM models and the average scores were converted into probabilities through comparison with active and inactive compounds score

distributions (validation set only), producing a measure of belonging to these two subsets.

The average score of the new compound was compared with active and inactive compounds scores and the active probability (Pa) was estimated from the fraction of active compounds with worse scores (Equation 1) and the inactive probability (Pi) was estimated from the fraction of inactive compounds with better scores (Equation 2) (Rocha et al. 2018).

$$Pa = \frac{FN}{N_a} = FNR \quad (1)$$

$$Pi = \frac{FP}{N_i} = FPR \quad (2)$$

Where N_a and N_i are the number of active compounds and the number of inactive compounds; FN is the number of active compounds with worse scores than the threshold; and FP is the number of inactive compounds with better scores than the threshold. The difference between the Pa and Pi (Pa-Pi) was used to evaluate the potential biological activity of modeled compounds.

The variance of Pa-Pi (σ^2_{Pa-Pi}) was analytically calculated from the sum of variances of Pa and Pi (Equations 3 and 4) and the confidence interval of Pa-Pi was calculated from the variance and Student *t*-value for a 95% confidence level (Equation 5), as described elsewhere (Rocha et al. 2018).

$$\sigma^2_{Pa-Pi} = \frac{var(Pa)}{N_a} + \frac{var(Pi)}{N_i} \quad (3)$$

$$\sigma^2_{Pa-Pi} = \frac{Pa*(1-Pa)}{N_a} + \frac{Pi*(1-Pi)}{N_i} \quad (4)$$

$$(Pa-Pi)_{estimate} = (Pa-Pi)_{mean} \pm t_{stat} * \sqrt{\sigma^2_{Pa-Pi}} \quad (5)$$

RESULTS AND DISCUSSION

The partial inclusion complex was prepared (93.5 % yield) using freeze drying method between [Ag(phen)$_2$]salH and β-CD in molar ratio 1:1. The FTIR, X-ray diffraction, TGA/DSC, ^{1}H and ^{13}C NMR and elemental analysis (CHN) data of [Ag(phen)$_2$] salH, β-CD, SIC [Ag(phen)$_2$]salH-β-CD and 1:1 SS of [Ag(phen)$_2$]salH with β-CD were compared.

FTIR results

The FTIR spectra of SIC, SS, β-CD and [Ag(phen)$_2$] salH are showed in Figure 1. In the IR spectrum of [Ag(phen)$_2$]salH (Fig. 1a) the broad absorption O-H band observed between 3200-3500 cm^{-1} shows the presence of water in the complex. The absorption band for the stretching of the O-H bond of the phenolic hydroxyl in SalH occurs around 3240 cm^{-1} but it is not observed in the spectrum. This is due to the absorption the water band are very broad and overlap one another. A sharp band at 3060 cm^{-1} was associated to the stretching vibration ν_s(=C-H) of the aromatic rings of the ligand 1,10-phenanthroline and the salicylate anion. Two bands at 2923 cm^{-1} and 2850 cm^{-1} were observed, indicating the formation of hydrogen bonds between the carbonyl group and the hydroxyl group of the salicylate anion (Banti et al. 2015). The absorption bands at 1586 cm^{-1} were correlated to the group (C=N) of 1,10-phenanthroline ligand and (C=O) of the salicylate anion at 1625 cm^{-1} (Gkaniatsou et al. 2015, Mujahid et al. 2016). Figure 1b shows the β-CD infrared spectrum, which has a broad band at 3384 cm^{-1} attributed to the stretchings ν_s(OH). An intense band at 2925 cm^{-1} assigned to the symmetric vibration ν_s(C-H) was observed, in addition to a band at 1644 cm^{-1} attributed to the deformation mode of the water included within the β-CD cavity. Bands of deformation modes δ(C-H) at 1417 cm^{-1} and 1368 cm^{-1} also appeared. The bands at 1157 cm^{-1} and 1029 cm^{-1} were

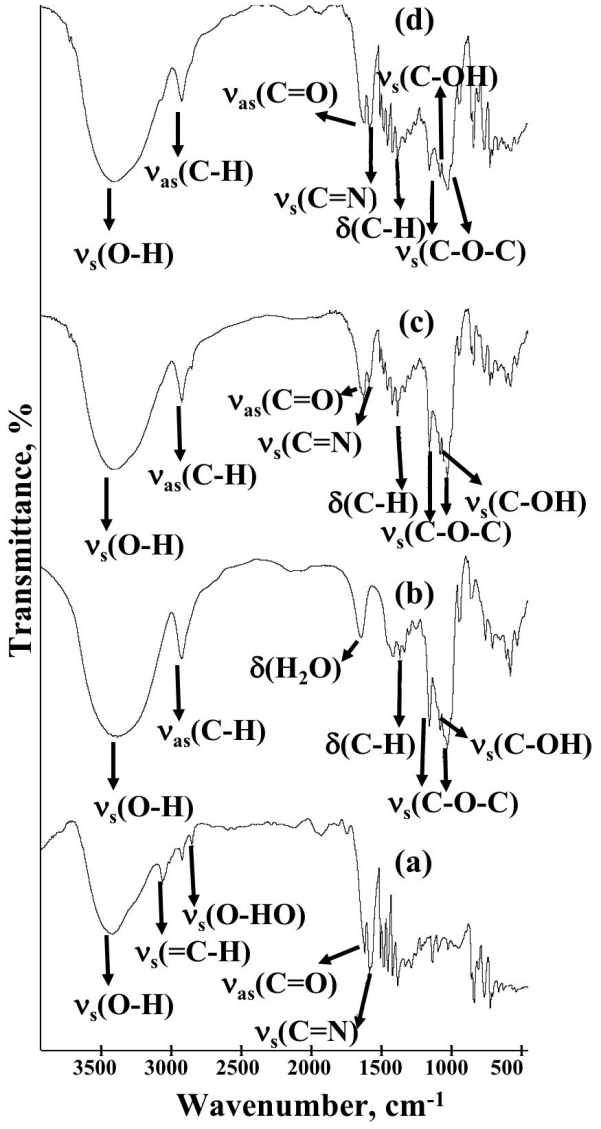

Figure 1. Absorption spectra (in KBr, cm^{-1}) in the infrared region of [Ag(phen)$_2$]salH (a), β-CD (b), solid inclusion complex [Ag(phen)$_2$]salH-β-CD (c) and 1:1 SS of [Ag(phen)$_2$]salH with β-CD (d).

attributed to the stretchings ν_s(C-O-C), and the band at 1080 cm^{-1} was assigned to the stretching ν_s(C-OH) (Burgos & Sinisterra 2010).

In the IR spectrum of SIC [Ag(phen)$_2$]salH-β-CD (Fig. 1c) and the 1:1 SS of [Ag(phen)$_2$]salH with β-CD (Fig. 1d), the characteristic absorption bands of β-CD and the silver(I) complex were observed varying in frequency, intensity and profile. These data indicate the presence of weak interactions, such as hydrogen bonds, between the compounds (Krishna et al. 2012, Vestland et al. 2015).

Based on Krishna et al. (2012), the band at 3406 cm^{-1} was assigned to ν_s(OH) stretching vibration of the SIC [Ag(phen)$_2$]salH-β-CD and corresponds to an overlap between the band at 3420 cm^{-1} (stretching ν_s(OH) of the salicylate anion) and the band at 3384 cm^{-1} (stretching ν_s(OH)) of the β-CD. These absorptions appeared by the process of inclusion of [Ag(phen)$_2$]salH (guest) in β-CD (host) through intermolecular interactions of hydrogen bonding. The band of the β-CD in 1644 cm^{-1} that corresponds to the mode of deformation (δ) of the water molecules was not observed in the SIC spectrum. These molecules are located in the cavity as inclusion waters and between the cyclodextrin molecules, as interstitial waters, maintaining the crystalline structure of the β-CD. In the partial inclusion compounds, when part of the molecule is included into the hydrophobic β-CD cavity no significant displacement of signal in the FTIR spectra is expected. The host-guest interaction is mediated by weak forces between molecules, such as hydrophobic interactions as van der Waals forces and hydrogen bonding (Burgos & Sinisterra 2010, Krishna et al. 2012) between the β-CD and [Ag(phen)$_2$]salH, when the compound of partial inclusion or association is formed.

No changes were observed in the frequency of the absorption band ν_s(C=N) of the ligand 1,10-phenanthroline. However, changes were observed in the band shift assigned to the stretching ν_{as}(C=O) of the salicylate anion of 1621 cm^{-1} to 1627 cm^{-1} in the SIC [Ag(phen)$_2$]salH-β-CD spectrum. This result shows partial inclusion or association of the guest molecule in β-CD. The band at 3060 cm^{-1} corresponding to the stretching ν_s(=C–H) in the silver complex, was not observed in the spectrum of the solid solution, due to the formation of new interactions

between the β-CD hydroxyl groups and the Ag(I) complex when the inclusion or association compound was formed in the solid state of SIC [Ag(phen)$_2$]salH-β-CD. In addition, the spectrum of 1:1 SS of [Ag(phen)$_2$]salH with β-CD presents a slight shift in the band of vibration ν_{as}(C=O), due to weak interactions when the partial inclusion complex is formed (Vestland et al. 2015). A decrease was also observed in the intensities of this band, as well as the band corresponding to the stretching ν_s(C=N), suggesting formation of new non-covalent interactions as van der Waals forces or hydrogen bonding when the association compound is formed between β-CD and [Ag(phen)$_2$]salH. This indicates that the SIC [Ag(phen)$_2$]salH-β-CD shapes new interactions between the ligand 1,10-phenanthroline with the groups (OH) located outside of the β-CD structure when the compound of association or partial inclusion is formed; and it was included inside the macromolecule of β-CD cavity through the aromatic ring of the salicylate anion (Stepniak et al. 2015).

Shifts were also observed in the absorption band of the SIC [Ag(phen)$_2$]salH-β-CD and 1:1 SS of [Ag(phen)$_2$]salH with β-CD, assigned to vibrations ν_{as}(C–H) of β-CD from 2925 cm^{-1} to 2934 cm^{-1}; the bands assigned to δ(C–H) of β-CD at 1417 cm^{-1} and 1368 cm^{-1} are shifted at 1422 cm^{-1} and at 1384 cm^{-1}, respectively. These results suggest the formation of a new supramolecular compound by hydrophobic interactions, dipole-induced dipole attraction and dipole-dipole forces (Stepniak et al. 2015, Das & Subuddhi, 2015) between the salicylate anion of the complex Ag(I) and the hydrogens located inside the cavity of the β-CD structure. Whereas, the phenanthroline ligand in the silver complex shapes an association compound by hydrogen bonds and van der Waals forces with the groups (OH) that are on the outside of the β-CD cavity (Burgos & Sinisterra 2010) indicating that in the solid state the compounds β-CD and [Ag(phen)$_2$]salH show host-guest interactions.

X-ray diffraction

The X-ray diffraction patterns of β-CD, [Ag(phen)$_2$]salH, 1:1 SS of [Ag(phen)$_2$]salH with β-CD and SIC [Ag(phen)$_2$]salH-β-CD are shown in Figure 2. The β-CD X-ray diffractogram (Fig. 2a) shows an intense peak at 2θ = 12.50° generated by its molecular structure cavity due to the head-to-head channel-type crystalline arrangement of the molecules of this compound, indicating the typical signals a polycrystalline diffraction pattern (Pradines et al. 2014). Figure 2b shows the [Ag(phen)$_2$]salH diffractogram with a diffraction pattern of crystalline nature presenting the most intense peak at 2θ = 24.29°.

When comparing the diffractograms of [Ag(phen)$_2$]salH and β-CD, with SIC [Ag(phen)$_2$]salH-β-CD (Figure 2c), the absence of signals may be seen corresponding to the X-ray diffraction patterns of the free compounds, in the position 2θ = 20.93° and 2θ = 22.78° of β-CD; and 14.49°, 15.53°, 24.29° and 26.66° of the silver(I) complex. New diffraction peaks appeared in the SIC [Ag(phen)$_2$]salH-β-CD, and their angles were 22.80°, 24.31°, 27.14° and 28.60°, revealing the favorable formation of this phase in the partial inclusion complex formed, in addition, the crystallinity of the inclusion compound decreases when compared to free compounds (Fig. 2a, b). These changes indicate that a different crystalline structure of the free compounds was generated, which was the partial inclusion complex, through van der Waals interactions, hydrogen bonds and hydrophobic interactions (Zou et al. 2014) between [Ag(phen)$_2$]salH and the cavity of the β-CD structure.

In the diffractogram of the SIC [Ag(phen)$_2$]salH-β-CD (Figure 2c), there are peaks corresponding to X-ray diffraction patterns of the free compounds, but with a significant reduction

of peak intensity as can be seen at position 2θ = 10.66°, 15.42°, 19.60° of β-CD and at position 2θ = 11.53° and 16.55° of [Ag(phen)$_2$]salH. These variations were caused by the formation of hydrogen bonds between the silver complex on the outside of the β-CD cavity, with a reduction in crystallinity. These observed differences indicate that the solid partial inclusion complex is formed due to the hydrophobic interaction of β-CD with the guest molecule (Burgos & Sinisterra 2010, Meinguet et al. 2015). These results corroborate with those found in FTIR spectroscopy by shifts in the absorption bands of the group (C=O) of the salicylate anion and (C=N) of the 1,10-phenanthroline ligand, after the inclusion phenomenon.

When comparing the diffractograms of the solid of partial SIC [Ag(phen)$_2$]salH-β-CD (Figure 2c) with the 1:1 SS of [Ag(phen)$_2$]salH with β-CD (Figure 2d), a superposition of spectra of the two substances is expected. However, minor shifts changes were observed, indicating that in the solid state [Ag(phen)$_2$]salH complex presents weak interactions with β-CD (Burgos & Sinisterra 2010, Pradines et al. 2014).

TGA/DSC results

The thermograms (TGA) of β-CD, [Ag(phen)$_2$]salH, 1:1 SS of [Ag(phen)$_2$]salH with β-CD and SIC [Ag(phen)$_2$]salH-β-CD are presented in Figure 3a. The TGA curve of β-CD (3aI) presented two characteristic thermal events (Wu et al. 2014, Garnero et al. 2014). The first one was observed

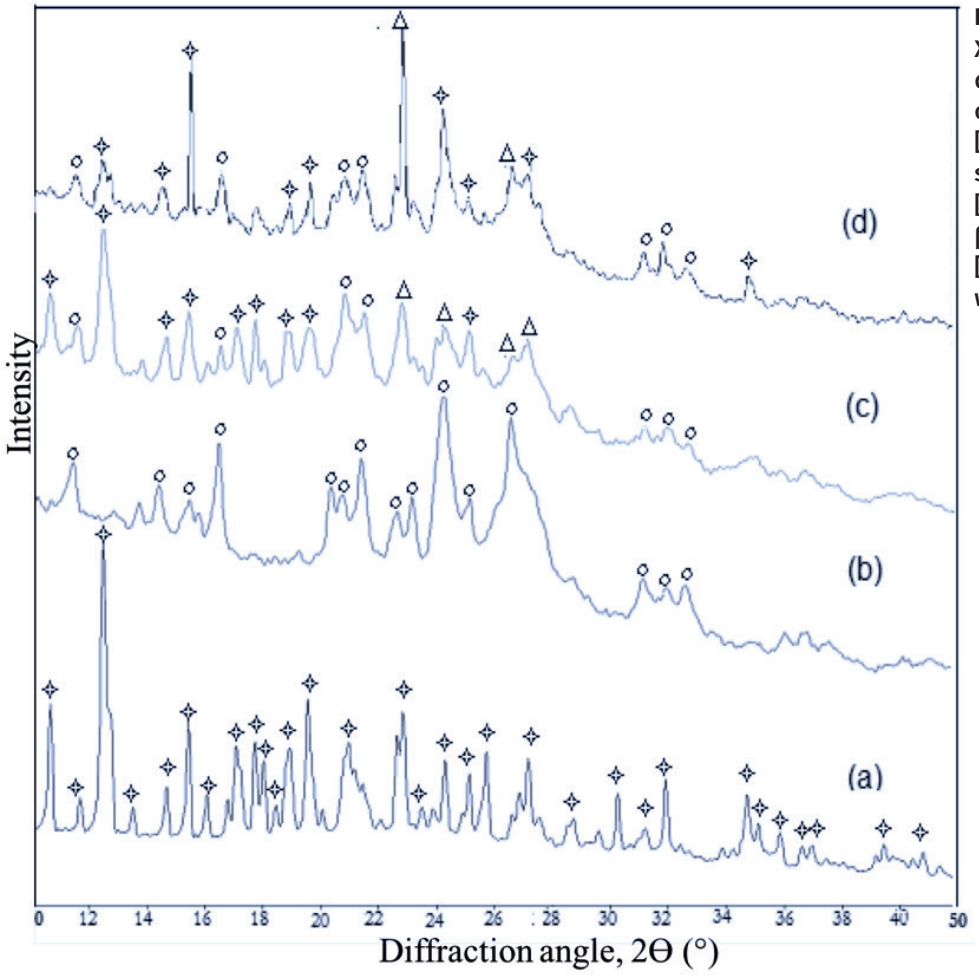

Figure 2. **X-ray powder diffractograms of β-CD (a), [Ag(phen)$_2$] salH (b), SIC [Ag(phen)$_2$]salH-β-CD (c), 1:1 SS of [Ag(phen)$_2$]salH with β-CD (d).**

between 60 °C and 110 °C with a maximum at 86.5 °C with about 11.6% of mass loss, corresponding to the departure of seven water molecules of the β-CD. These water molecules are located within the cavity of the β-CD chemical structure, as inclusion water, and between the cyclodextrin molecules, as interstitial water, maintaining the β-CD crystal structure (Burgos & Sinisterra 2010). Then, the TGA curve shows thermal stability (110 °C and 285 °C). The second thermal event, between 285 °C and 341 °C with a maximum at 320 °C, was attributed to the decomposition of the glycosidic ring β-CD and char formation (Sinniah et al. 2015) with about 66% of mass loss. A similar phenomena was verified in the DSC curve (Figure 3a, b) at 86.5 °C and 320 °C, as endothermic events, due to the loss of water molecules and the decomposition of the β-CD.

In the TGA curve of compound [Ag(phen)$_2$] salH (Figure 3a), a first thermal event between 27.8 °C and 90.5 °C was observed with a maximum at 46 °C and 3% of mass loss attributed to the moisture of the silver(I) complex (with 1H$_2$O). From 90 °C to 228 °C, the compound presented thermal stability, and between 235 °C and 315 °C it presented a second thermal event related to the decomposition of the metal complex with 84% of mass loss (Duarte et al. 2015). In the DSC curve of [Ag(phen)$_2$]salH (Figure 3b), a first endothermic event was observed at 45 °C, related to dehydration of the metal complex. An important feature in this event is that the endothermic signal of the complex dehydration is composed of two signals: at temperatures 45 °C and 73 °C, two different heat absorptions were observed during dehydration of the complex. A second and third endothermic process were also observed with a peak at 246 °C and 285 °C respectively, related to the melting and decomposition point of the compound. There was a fourth thermal event at 460 °C through an exothermic process, indicating the formation of metallic Ag directly by the thermal decomposition of silver acetate, that tend to the formation of silver nanoparticles (Ag-NPs) (Nakano et al. 2016).

In the TGA curve of SIC [Ag(phen)$_2$]salH-β-CD and 1:1 SS of [Ag(phen)$_2$]salH with β-CD, (Figure 3aIII, and 3aIV respectively). A first thermal event was observed between 40 °C and 93 °C with 7.5% of mass loss, corresponding to the departure of 7 water molecules due to dehydration of the metal complex, and departure of the water molecules from the cavity and the interstices of the β-CD crystal structure (Pradines et al. 2014). These results confirm the formation of the partial inclusion complex [Ag(phen)$_2$]salH within the β-CD cavity via hydrophobic interactions, van der Waals forces, and hydrogen bonds (Duarte et al. 2015), as observed in the results of FT-IR spectroscopy of SIC [Ag(phen)$_2$]salH-β-CD which indicated the presence of host-guest interactions between [Ag(phen)$_2$]salH and β-CD.

The SIC [Ag(phen)$_2$]salH-β-CD is stable between 95 °C and 215 °C. Moreover, between 235 °C and 265 °C, a thermal decomposition event was observed with 19.8% of mass loss. This temperature range coincides with the beginning of the decomposition temperature of [Ag(phen)$_2$]salH and β-CD, suggesting stability in the inclusion complex. Additionally, when comparing the TGA curves of SIC [Ag(phen)$_2$] salH-β-CD, 1:1 SS of [Ag(phen)$_2$]salH with β-CD, [Ag(phen)$_2$]salH and β-CD, it can be seen that the inclusion or association compound has less thermal stability with respect to the free silver(I) complex.

The DSC curve of the SIC [Ag(phen)$_2$]salH-β-CD (Figure 3b, c) showed two endothermic events and one exothermic event. The first one with a temperature at 76 °C corresponds to the departure of hydration water molecules from the silver(I) complex, and to the inclusion water in the β-CD cavity. The second endothermic

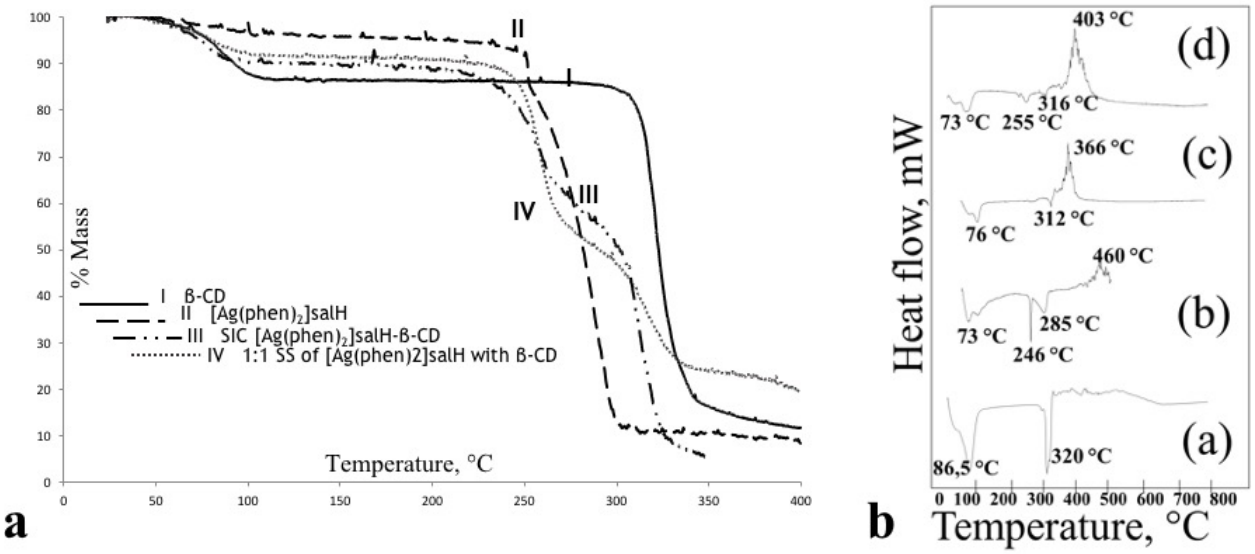

Figure 3. a - TGA results of β-CD (I), [Ag(phen)$_2$]salH (II), 1:1 SS of [Ag(phen)$_2$]salH with β-CD (III) and SIC [Ag(phen)$_2$] salH-β-CD (IV). b - DSC results of β-CD (a), [Ag(phen)$_2$]salH (b), SIC [Ag(phen)$_2$]salH-β-CD (c) and 1:1 SS of [Ag(phen)$_2$]salH with β-CD (d). The amount of sample used was 2.5 mg, in an alumina capsule and in a dynamic atmosphere of nitrogen. The heating rate was 10 °C min^{-1}.

event at 312 °C was attributed to the β-CD decomposition. A third thermal event observed at 366 °C, was related to the silver oxidation (exothermic process). This thermal process, compared to that of the free complex [Ag(phen)$_2$] salH (460 °C), reveals the changes in the thermal properties of the metal complex by the presence of host-guest interactions with β-CD when the inclusion complex is formed (Burgos & Sinisterra 2010). The DSC curve for the mechanical mixture of [Ag(phen)$_2$]salH and β-CD, presented similar results to those shown in the DSC curve of the inclusion complex, confirming the presence of host-guest interactions between [Ag(phen)$_2$]salH and β-CD in the solid state by van der Waals forces and hydrogen bonds (Zhang et al. 2015, Zhu et al. 2016, Da Rosa et al. 2013).

In general, studies on thermal decomposition reported the presence of host-guest interactions between β-CD and the silver(I) complex, which confirms the obtaining of the partial SIC [Ag(phen)$_2$]salH-β-CD. This compound has low thermal stability in relation to the free compound [Ag(phen)$_2$]salH, owing the formation of non-covalent interactions such as hydrogen bonds and van der Waals forces between a fraction of [Ag(phen)$_2$]salH and the exterior of the β-CD cavity.

^{1}H NMR results

The chemical shifts assignments (δ) observed in the ^{1}H NMR spectra (DMSO-d$_6$, 400 MHz) of β-CD and the SIC [Ag(phen)$_2$]salH-β-CD are presented in Table I (Figs. S1-S7). Small changes were observed in the chemical shifts of all β-CD hydrogens (Figure 4a). The chemical shifts for the H-2 and H-4 protons ($\Delta\delta$ = 0.026 ppm and 0.027 ppm, respectively), which are located at the exterior side of the β-CD cavity, are slightly higher compare to other protons. This allows supposing the formation of host-guest hydrogen bonds in the outside of β-CD cavity, showed down-field changes. Moreover, the H-3 ($\Delta\delta$ = 0.002 ppm) and H-5 ($\Delta\delta$ = 0.005 ppm), located in the inner of hydrophobic cavity of β-CD exhibit small chemical shifts. Besides, chemical shifts are the result of the induced effect by the ring current effect of the aromatic

part of the silver complex [Ag(phen)$_2$]salH-β-CD. These results indicate that one part of the guest molecule is inside the β-CD cavity and another part outside the cavity forming the host-guest partial inclusion compound (Burgos & Sinisterra 2010, Yang et al. 2013).

The chemical shifts (δ) of the [Ag(phen)$_2$] salH were compared with those of the SIC [Ag(phen)$_2$]salH-β-CD (Table I). Small variations were observed in the δ values of all hydrogens of the [Ag(phen)$_2$]salH in relation to the SIC, which are more pronounced for the protons H-2´, H-7´ and H-3´, H-6´ (Δδ= 0.013 ppm and 0.012 ppm, respectively) of the 1,10-phenanthroline ligand. These results suggest the formation of new interactions such as van der Waals forces and hydrogen bonds that form in the external part of the β-CD cavity, through the primary and secondary hydroxyl groups, when the partial inclusion compound is formed or compound of association between β-CD and [Ag(phen)$_2$]salH. The H-f proton corresponding to the salicylate anion, showed a high-field chemical shift (Δδ = 0.009 ppm) through molecular screening of β-CD on this proton, showing that the salicylate anion was entirely included within the hydrophobic β-CD cavity (Moyano et al. 2012, Wang et al. 2015). Chemical shifts towards high-field signals of protons H-c (Δδ = 0.004 ppm), H-d and H-e (Δδ = 0.002 ppm) of the salicylate anion show host-guest interactions between β-CD and [Ag(phen)$_2$] salH, caused by the hydrophobic environment of the β-CD cavity, suggesting hydrogen bond type interactions and van der Waals forces, when the anion enters the β-CD cavity. These changes

Table I. ^{1}H NMR data (400 MHz, DMSO-d$_6$) of β-CD, [Ag(phen)$_2$]salH and solid inclusion complex [Ag(phen)$_2$] salH-β-CD.

Hydrogen	δ [ppm]			
	β-CD	[Ag(phen)$_2$]salH	[Ag(phen)$_2$]salH-β-CD	Δδ
H-1	4.824	-	4.828	0.004
H-2	3.312	-	3.338	0.026
H-3	3.635	-	3.633	-0.002
H-4	3.350	-	3.377	0.027
H-5	3.554	-	3.549	-0.005
H-6 (2H)	3.664	-	3.662	-0.002
H-d, H-e (2H)	-	6.540	6.542	0.002
H-c	-	7.106	7.110	0.004
H-f	-	7.638	7.629	-0.009
H-2´, H-7´ (4H)	-	7.991	8.004	0.013
H-4´, H-5´ (4H)	-	8.218	8.218	0.000
H-3´, H-6´ (4H)	-	8.764	8.776	0.012
H-1´, H-8´ (4H)	-	9.157	9.161	0.004

$\Delta\delta = \delta_{\text{inclusion compound}} - \delta_{\text{free compound}}$; negative values indicate high-field chemical shifts, and positive values correspond to low-field chemical shifts.

suggest partial inclusion of the guest molecule as depicted in Figure 4.

^{13}C NMR results

The chemical shift assignments (δ) observed in the ^{13}C NMR spectra (DMSO-d$_6$, 100 MHz) of β-CD and the SIC [Ag(phen)$_2$]salH-β-CD are presented in Table II. There are characteristic signals of carbon nuclei of the silver compound and of β-CD. Changes were observed in the chemical shifts of the metal complex carbon atoms. These changes are associated with weak non-covalent interactions such as van der Waals forces (Najlaouia et al. 2015) among Ag(I) complex and the β-CD. Comparing the β-CD and the SIC [Ag(phen)$_2$]salH-β-CD ^{13}C-NMR spectra, low-field chemical shifts were observed in all signals of the β-CD carbon nuclei in the inclusion compound. The most representative changes were for C-2 (Δδ = 0.02 ppm), C-1, C-3, C-5 and C-6 with Δδ = 0.01 ppm. These results indicate that the partial inclusion complex was formed through the secondary hydroxyl groups of the β-CD molecule, on the broad side of the truncated cone of the macrocycle structure, forming a compound with a topology of partial inclusion and association (Limaa et al. 2016, Ho et al. 2016).

Comparing the [Ag(phen)$_2$]salH and the SIC [Ag(phen)$_2$]salH-β-CD ^{13}C NMR spectra, small variations were observed in the high-field chemical shifts of the signals of carbons C-c, C-e (Δδ = 0.09 ppm) and C-d (Δδ = 0.29 ppm) of the salicylate anion. These results suggest that the salicylate anion enters the β-CD cavity, forming the partial inclusion compound by new weak noncovalent interactions (Moyano et al. 2012, Da Rosa et al. 2013, Billes et al. 2013). Variations were also observed in the low-field chemical shifts in the signals of all carbon nuclei of the ligand, probably because the hydroxyl groups outside the β-CD form intermolecular interactions van der Waals forces (Korytkowska-Wałach et al. 2017) with the metal complex [Ag(phen)$_2$]salH. The aromatic ring of the salicylate is completely inside the hydrophobic cavity of the β-CD and the C-d carbon is forming weak van der Waals forces or hydrogen bonding interactions with the H-3 and H-5 or from the outside through the primary hydroxyl of β-CD (Figure 4).

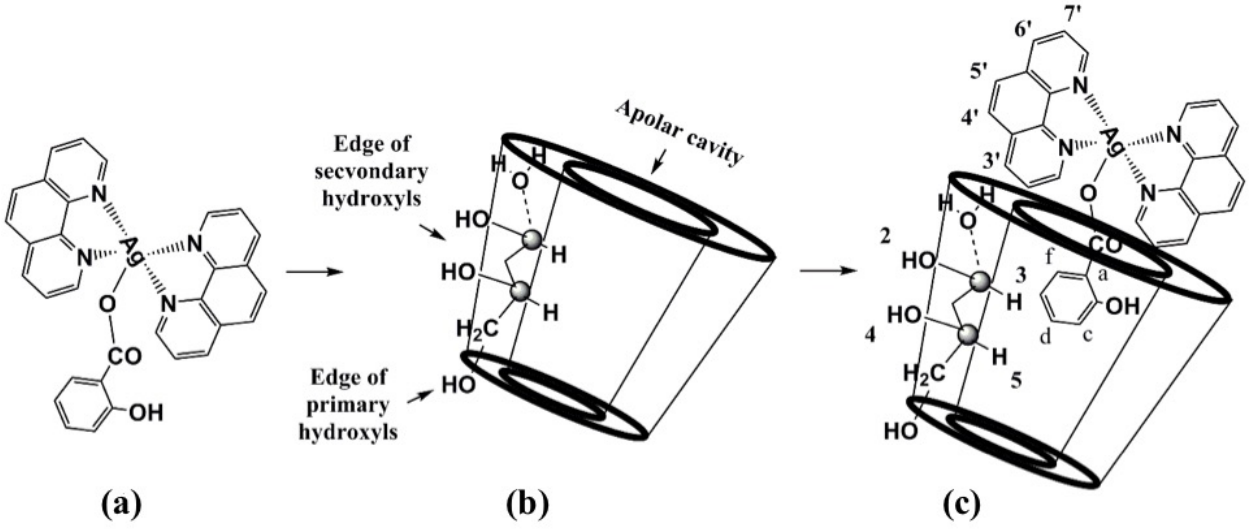

Figure 4. Schem of partial inclusion of bis(1,10-phenanthroline)silver(I) salicylate (a) in apolar cavity of β-cyclodextrin (b) producing the partial inclusion complex (c).

COSY experiment

The COSY experiment shows the homonuclear correlation of the hydrogens in the partial inclusion complex [Ag(phen)$_2$]salH-β-CD (Fig. S8). The presence of signals that correlate to the aromatic ring hydrogens of the salicylate anion of the Ag(I) compound with the hydrogens located inside the cavity of the β-CD chemical structure was observed. These results confirm the partial inclusion of [Ag(phen)$_2$]salH within the β-CD. Signal correlations of 1,10-phenanthroline hydrogen atoms with hydrogens (H-2 and H-4) atoms found in the exterior of the macrocycle truncated cone structure were caused by associated interactions between [Ag(phen)$_2$] salH and β-CD, including hydrogen bonds and van der Waals forces.

The results obtained by ^{1}H and ^{13}C NMR spectroscopy, suggests partial inclusion topology of [Ag(phen)$_2$]salH within the β-CD (Figure 4). This inclusion occurred through the interaction of hydrogen H-5 of β-CD with hydrogens H-d and H-e of the aromatic ring of the salicylate anion. In addition, the hydrogen interactions between H-3 of β-CD and H-f of the salicylate anion and between the hydrogens H-6 of β-CD with H-c of the salicylate anion, indicate that the anion is completely included in the hydrophobic β-CD cavity.

In the COSY spectra of SIC [Ag(phen)$_2$] salH-β-CD it was observed that the β-CD, H-1 interacts with hydrogens H-1´ and H-8´ of the ligand 1,10-phenanthroline, and H-2 of β-CD with H-2´ and H-7´. The hydrogen H-3´ and H-6´

Table II. ^{13}C NMR data (100 MHz, DMSO-d$_6$) data of β-CD, [Ag(phen)$_2$]salH and solid inclusion complex [Ag(phen)$_2$] salH-β-CD.

Carbon	δ [ppm]			
	β-CD	[Ag(phen)$_2$]salH	[Ag(phen)$_2$]salH-β-CD	Δδ
C-1	101.82	-	101.83	0.01
C-2	72.30	-	72.32	0.02
C-3	72.93	-	72.94	0.01
C-4	81.44	-	81.44	0.00
C-5	71.92	-	71.93	0.01
C-6	59.81	-	59.82	0.01
C-c, C-e	-	115.71	115.62	-0.09
C-d	-	131.30	131.01	-0.29
C-f	-	129.78	129.80	0.02
C-2´, C-7´	-	124.72	124.75	0.03
C-4´, C-5´	-	127.03	127.08	0.05
C-3´, C-6´	-	138.18	138.20	0.02
C-1´, C-8´	-	151.16	151.11	0.05
C-9´, C-10´	-	142.04	142.14	0.10
C-11´, C-12´	-	128.83	128.89	0.06

$\Delta\delta = \delta_{\text{inclusion compound}} - \delta_{\text{free compound}}$; negative values indicate high-field chemical shifts, and positive values correspond to low-field chemical shifts.

of 1,10-phenanthroline correlates with H-6 of β-CD (Fig. S8). No correlation was observed between hydrogen H-4´ and H-5´ of the ligand 1,10-phenanthroline with β-CD hydrogen atoms. Therefore, the full inclusion of the aromatic ring of the salicylate anion within the cavity of the macrocycle truncated conical structure of β-CD is performed through the broad base in which the secondary hydroxyl groups OH-2 and OH-3 are located (Figure 4).

Thus, the partial inclusion complex [Ag(phen)$_2$]salH-β-CD was successfully prepared using a freeze drying method between [Ag(phen)$_2$] salH and β-cyclodextrin in a molar ratio 1:1. The results obtained by FTIR, elemental analysis, TG/DSC, ^{1}H and ^{13}C NMR and XRD, characterized the partial inclusion compound.

In vitro antimicrobial activity

Lower antifungal activity of $AgNO_3$, 1,10-phenanthroline (phen), [Ag(phen)$_2$]salH and [Ag(phen)$_2$]salH-β-CD was observed when compared with the positive control of Cotrimazol® (Table III). In addition, $salH_2$ did not present activity in microorganism growth control. When comparing the growth inhibition halos of *C. albicans* with $AgNO_3$ and [Ag(phen)$_2$] salH, similar inhibition halos (10-12 mm) were observed, suggesting that the activity of the silver(I) complex occurs due to the presence of cations (Ag^+), which, right after entering the cells, induce apoptosis by disruption of the mitochondrial function and DNA fragmentation (Mujahid et al. 2016).

The antifungal effect of [Ag(phen)$_2$]salH can also be related to the action of the ligand 1,10-phenanthroline (which is also active) because it provides a lipophilic character to the cations (Ag^+), promoting the permeability of the coordination compound through the lipid layer of the cell membrane (Wu et al. 1999) fragmentation and inhibition of the DNA synthesis by intercalation processes (Deegan et al. 2007). Thus, the cation [Ag(phen)$_2$]$^+$, due to its low charge density and flat spatial structure, is an antibacterial active part of the silver(I) complex (Moyano et al. 2012) having intercalation interactions with the DNA chain, inducing apoptosis (Deegan et al. 2007, Zhu et al. 2016).

The antimicrobial activity and bioavailability of [Ag(phen)$_2$]$^+$ were improved with the inclusion of the [Ag(phen)$_2$]salH into the β-CD since the permeability of microorganisms caused by host-guest interactions between the β-CD and the cell membrane phospholipids increased (Duarte et al. 2015). This facilitated the incorporation, transport and bioavailability of [Ag(phen)$_2$]$^+$ in the cellular system (Terauchi et al. 2016), thus allowing for antifungal action mechanism of [Ag(phen)$_2$]salH with interruptions in the mitochondrial functions and interactions with DNA (Moyano et al. 2012).

In silico prediction of antimicrobial activity

Using the procedure described in the Experimental Section, we have developed 49 predictive SVM models, which are described in the (Table SI- Supplementary Material) together with their internal validation using AUC-ROC as a figure-of-merit. We have modeled a total of 27 datasets for *C. albicans* composed of 24 cell based assays and 3 biochemical enzyme inhibition assays. The average AUC was 0.61, which is good bearing in mind that most are related to cell based assays. These models have an average of 702 compounds and 250 active compounds. Regarding *P. aeruginosa* a total of 18 datasets were modeled with an average AUC of 0.72, a very good result for cell based assays, with a mean of 388 compounds and 140 active compounds. For *S. auereus* we have modeled 4 datasets, with an mean AUC of 0.60 and an average of 6379 compounds with 87 active

Table III. Inhibition of bacterial and fungal growth by solutions of cotrimazol® (1 mM) $AgNO_3$ (500 µM) 1,10-phenanthroline; [Ag(phen)$_2$]salH (500 µM) and [Ag(phen)$_2$]salH-β-CD (500 µM).

Compound	Growth inhibition halo [mm]		
	Staphylococcus aureus	***Pseudomonas aeruginosa***	***Candida albicans***
$AgNO_3$	7±2.1	7±0.8	10±14
1,10-phenanthroline	9±2.1	7±0.8	12±14
[Ag(phen)$_2$]salH	8±2.9	8±1.6	12±1.6
[Ag(phen)$_2$]salH-β-CD	10±1.0	10±2.1	15±08
Cotrimazol®	21±2.1	11±2.1	20±20

compounds. Only 39 models with an AUC higher than 0.5 were used in the subsequent steps.

Before to being able to perform the predictions about 1,10-phenanthroline biological activities, we first made an ultimate validation using some known activities of this compound and other 2 analogues, one dimethyl derivative and one 8-aminoquinolyl analog (Figure 5). These compounds were tested in the projects "Reversing Antifungal Drug Resistance Project" (PubChem Bioassay summary AID=2007) from the Broad Institute and "Probe development efforts to identify selective inhibitors of VIM-2 metallo-beta-lactamase" (PubChem Bioassay summary AID=1854) from The Scripps Research Institute Molecular Screening Center.

The experimental outcomes for 1,10-phenanthroline (PubChem Compound CID=1318), 2,9-Dimethyl-1,10-phenanthroline (PubChem Compound CID=65237) and 7-methylquinolin-8-amine (PubChem Compound CID=231556) are shown in (Table SII). These 3 compounds appear as active or inactive in 9 modeled datasets, totalizing 11 occurrences. Before proceeding to the modeling and validation steps these compounds were excluded and the remaining compounds were used to build a model ensemble for each dataset. The values of Pa-Pi were used to rank the activities and the Matthews Correlation Coefficient (MCC) (Boughorbel et al. 2017) was the metric of choice to establish the threshold value above which the compound is predicted to be active. The cutoff of Pa-Pi ≥ 0.05 was revealed to be the optimal value as it produced a MCC of 0.41, with a sensitivity of 0.8 and a specificity of 0.5. With a cutoff of Pa-Pi ≥ 0.15, the MCC drops to 0.35 and the sensitivity goes to 0.6 and the specificity to 0.67.

Once the threshold value was established, we selected all biological activities in which the 1,10-phenanthroline was predicted to be active. From 49 modeled datasets, the 1,10-phenanthroline was predicted to be active in 18 (Table IV), being 8 for *C. albicans*, 9 for *P. aeruginosa* an 1 for *S. aureus*. The most prominent predictions occur with *C. albicans* targets calcineurin (PubChem Bioassay AID=2388) and Rtt109 (PubChem Bioassay AID=588764) with Pa-Pi values of 0.659 and 0.781, respectively. These targets are very promising against multi-drug resistance pathogens. The calcineurin is a conserved Ca^{2+}-calmodulin-activated, serine/threonine-specific protein phosphatase that regulates a variety of physiological processes, e.g., cell cycle progression, polarized growth,

and adaptation to salt and alkaline pH stresses (Bader et al. 2003). The calcineurin A (CNA) of *C. albicans* is involved in antifungal tolerance, cell morphogenesis and virulence (Reedy et al. 2010). The Rtt109-Vps75 is unique to fungii such as *C. albicans* and it is associated with both resistance to genotoxic stress and pathogenesis (Rosa et al. 2010, D'Arcy & Luger 2011). It could be a viable route to a novel antifungal, which may work alone, or in combination with existing anti-fungal treatments. Other potential targets for 1,10-phenanthroline, related to *C. albicans* activity, are TPT1 (tRNA 2'-phosphotransferase) and RNAse T1 (Ribonuclease T1) which can revoke drug resistance in diverse fungi including species of *Candida* (Cowen & Lindquist 2005). The TPT1 can be found in yeast and humans (Culver et al. 997), however, some studies suggest that the gene is nonessential in mammals. As a result, the identification of selective inhibitors of TPT1 could reveal potential anti-fungal agents (Harding et al. 2008). The RNAse T1 is a fungal endonuclease that cleaves single-stranded RNA after guanine residues (Pace et al. 1991, Olombrada et al. 2017), therefore, also, it could be a good target for an antifungal agent.

In the case of *P. aeruginosa* most of the 9 activity models where 1, 10-phenanthroline is predicted to be active are related to the inhibition of VIM-2 and IMP-1 metallo beta-lactamase (Nordmann et al. 2011). The maximum values of Pa-Pi for VIM-2 and IMP-1 were 0.502 (PubChem Bioassay AID=2754) and 0.391 (PubChem Bioassay AID=2756), respectively. Metallo-β-lactamases are a diverse set of enzymes that catalyze the hydrolysis of a broad range of β-lactam drugs including carbapenems (Palzkill 2013). Metallo-β-lactamases have attracted considerable attention due to their role in microbial resistance to β-lactam antibiotics (Siemann et al. 2002).

For *S. aureus* the only model to which the 1,10-phenanthroline was predicted to be active is related to the bacterial quorum sensing (PubChem Bioassay AID=527) with a Pa-Pi value of 0.581. The quorum sensing (QS) is a process of cell-cell communication that allows bacteria to share information about cell density and adjust gene expression accordingly. This process involves the production, detection, and response to extracellular signaling molecules. Among the many traits controlled by quorum sensing is the expression of virulence factors by pathogenic bacteria such as sporulation, competence, antibiotic production, biofilm formation, and virulence factor secretion (Rutherford & Bassler 2012).

As stated above, in the ligand-based approach selected to perform the prediction it was not possible to make predictions about the silver complex, because it depends on the

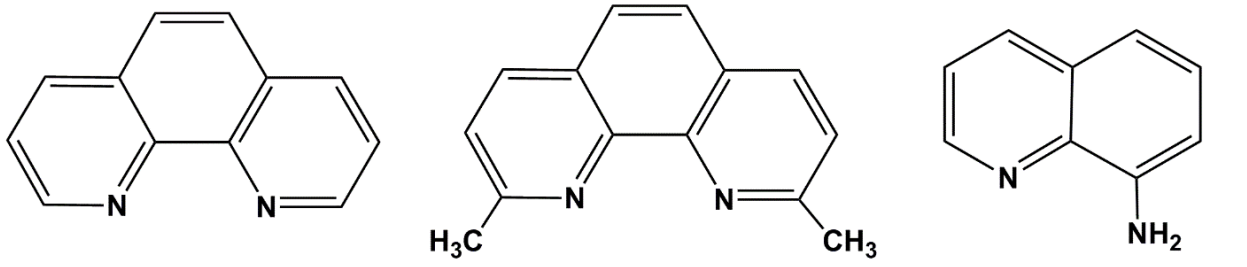

Figure 5. Chemical structure of compounds used to validate the SVM models.

Table IV. Models were the 1,10-phenanthroline (AID=1318) was predicted to be active by SVM modeling. The Pa-Pi cutoff value of 0.05 was used to make the predictions. When available the experimental results for 1,10-phenanthroline (CID=1318), 2,9-Dimethyl-1,10-phenanthroline (CID=65237) and 7-methylquinolin-8-amine (CID=231556) were included for comparison purposes.

Organism	PubChem Bioassay		SVM Modeling		Experimental Outcome		
	AID [a]	Title	Pa-Pi [b]	Predicted Outcome	1318 [c]	65237 [c]	231556 [c]
C. albicans	2467	Fluorescence Cell-Based Retest of *C. albicans* Growth in the Presence of Fluconazole	0.216±0.032	Active	Inactive	Active	
C. albicans	2423	Fluorescence Cell-Based Secondary Assay to Identify Inhibitors of Resistant *C. albicans* Growth in the Presence of Fluconazole	0.055±0.039	Active	Active	Active	
C. albicans	488807	Antifungal Drug Resistance - Resistant Strain Measured in Microorganism System Using Plate Reader - 2037-02 Inhibitor Dose DryPowder Activity	0.100±0.190	Active			
C. albicans	2400	Luminesence Cell-Based Secondary Assay to Identify Inhibitors of Hsp90	0.117±0.073	Active		Inactive	
C. albicans	2388	Luminesence Cell-Based Secondary Assay to Identify Inhibitors of Calcineurin	0.659±0.122	Active		Inactive	
C. albicans	2149	Fluorescence polarization-based biochemical high throughput confirmation assay to identify inhibitors of tRNA 2'-phosphotransferase (TPT1).	0.110±0.029	Active			
C. albicans	2153	Fluorescence polarization-based counterscreen assay for inhibitors of tRNA 2'-phosphotransferase (TPT1): biochemical high throughput screening assay to identify inhibitors of RNAse T1.	0.187±0.033	Active			
C. albicans	588764	Rtt109/Vps75 Measured in Biochemical System Using Plate Reader - 2106-01 Inhibitor Dose CherryPick Activity	0.781±0.055	Active			
P. aeruginosa	1860	Epi-absorbance-based confirmation biochemical high throughput screening assay to identify selective inhibitors of VIM-2 metallo-beta-lactamase.	0.423±0.092	Active			
P. aeruginosa	2187	Epi-absorbance-based confirmation assay for common VIM-2 and IMP-1 inhibitors: biochemical high throughput screening assay to identify inhibitors of VIM-2 metallo-beta-lactamase.	0.177±0.083	Active			Active

Table IV. (continuation)

Organism	PubChem Bioassay		SVM Modeling		Experimental Outcome		
	AID [a]	Title	Pa-Pi [b]	Predicted Outcome	1318 [c]	65237 [c]	231556 [c]
P. aeruginosa	2189	Epi-absorbance-based confirmation assay for common IMP-1 and VIM-2 inhibitors: biochemical high throughput screening assay to identify inhibitors of IMP-1 metallo-beta-lactamase.	0.137±0.090	Active			
P. aeruginosa	2184	Epi-absorbance-based counterscreen assay for common VIM-2 and IMP-1 inhibitors: biochemical high throughput screening assay to identify inhibitors of TEM-1 serine-beta-lactamase.	0.093±0.081	Active			
P. aeruginosa	2756	Epi-absorbance-based dose response assay for common IMP-1 and VIM-2 inhibitors: biochemical high throughput screening assay to identify inhibitors of IMP-1 metallo-beta-lactamase	0.391±0.151	Active			
P. aeruginosa	2754	Epi-absorbance-based dose response assay for common IMP-1 and VIM-2 inhibitors: biochemical high throughput screening assay to identify inhibitors of VIM-2 metallo-beta-lactamase	0.502±0.127	Active			
P. aeruginosa	2755	Epi-absorbance-based dose response assay for common IMP-1 and VIM-2 inhibitors: biochemical high throughput counterscreen to identify inhibitors of TEM-1 metallo-beta-lactamase	0.332±0.125	Active			
P. aeruginosa	Several	Inhibitors of VIM-2 metallo-beta-lactamase	0.411±0.047	Active			
P. aeruginosa	493231	Fluorescent Biochemical Primary HTS to Identify Inhibitors of P. aeruginosa PvdQ acylase Measured in Biochemical System Using Plate Reader and Imaging Combination - 2091-01 Inhibitor Dose CherryPick Activity	0.147±0.060	Active			
S. aureus	527	Primary HTS Assay For Inhibitors Of Bacterial Quorum Sensing	0.581±0.077	Active			

[a]PubChem BioAssay Identifier (AID) of the datasets;
[b]Diference between the probability of being active (Pa) or inactive (Pi).
[c]PubChem Compound Identifier (CID) of the compounds.

datasets available and the set of descriptors used. However, it is possible to infer that the inclusion complex probable improves the pharmacokinetics properties such as permeability of the compound, but not the pharmacodynamics characteristics. The antimicrobial activity of the free-ligand and its silver complex are too close to stated that one is better than other (Table III). According to the biological results, the antifungal activities of the compound reside on the effect of the silver complex and/or on the free-ligand itself over biological targets of the pathogenic organisms. The *in silico* predictions allow us to infer the putative targets that could be responsible for the antimicrobial activity, like RTT and calcineurin for *C. albicans*, or metallo-β-lactamases for *P. aeruginosa* or bacterial quorum sensing in the case of *S. aureus*. These results would not be achievable unless we had performed a large number of set of biological tests that is inaccessible at this moment. Furthermore, the *in silico* analysis opens new possibilities for further studies considering the pharmacological activities predicted for the ligand that can be related with the silver complexes. The present results can contribute to an increase in our knowledge about the probable biological targets.

In summary, a new compound of partial inclusion between bis(1,10-phenanthroline) silver(I) salicylate and β-cyclodextrin in 1:1 molar ratio was prepared. The results obtained by the different analytical techniques used in this study, showed considerable variations that allow us to suggest the formation of a compound of partial inclusion between host-guest. The compound evaluated by *in silico* method showed an antimicrobial activity against *C. albicans*, *P. aeruginosa* and *S. aureus* through different potential mechanisms of action which could be explored to develop new antifungal and antibacterial drugs. It is important to emphasize that these microorganisms have clinical relevance considering the associated diseases and the increase resistance to antibiotics. Other important aspects of this *in silico* study is that the majority of predicted targets are related to a virulence factors and/or resistance of strains.

CONCLUSION

The partial inclusion complex [Ag(phen)$_2$] salH-β-CD shows a higher activity than free compounds, that could be related to a higher bioavailability of [Ag(phen)$_2$]$^+$, but a more reduced activity than clotrimazole in the tested microorganisms. The presence of cations (Ag^+), which can induce apoptosis by disruption of the mitochondrial function and DNA fragmentation, and the increased permeability of a coordination compound through the lipid layer of the cell membrane are possible mechanisms of action. The increased permeability can cause inhibition of DNA synthesis by intercalation of the silver complex with DNA. In addition, the *in silico* studies using the SVM machine learning method suggested the activity of compounds active against *C. albicans*, *P. aeruginosa* and *S. aureus* might be related to several biological targets associated with the drug-resistance of pathogens other factors that contribute to fungi and bacteria pathogenicity. These factors could also contribute to antimicrobial activity of 1,10-phenanthroline and eventually the silver complex.

Data availability

Additional data about *in silico* models used to support the findings of this study are available from the JCD Lopes (jlopes.ufmg at gmail.com) upon request.

Acknowledgments

The authors thanks to Universidad Nacional de Colombia, Sede Bogotá, for the financial support for AEBC (Division de Investigación - Sede Bogotá, DIB Research Projects No. 201010029091 and 201010029302), and the Conselho Nacional de Desenvolvimento Científico e Tecnológico (CNPq) for the fellowship of JCD Lopes [202407/2014-4] and VL Almeida [249299/2013-5] in the Science Without Borders program. The authors are also grateful to to Prof. Sidney Augusto Vieira Filho for the revision of the manuscript and for many valuable suggestions.

REFERENCES

BADER T, BODENDORFER B, SCHRÖPPEL K & MORSCHHÄUSER J. 2003. Calcineurin is essential for virulence in *Candida albicans*. Infect Immun 71(9): 5344-5354.

BANTI CN, GIANNOULIS AD, KOURKOUMELIS N, OWCZARZAK AM, KUBICKI M & HADJIKAKOU SK. 2015. Silver(I) compounds of the anti-inflammatory agents salicylic acid and p-hydroxyl-benzoic acid which modulate cell function. J Inorg Biochem 142: 132-144.

BILLES F, HERNANZ A, MIKOSCH H & BRATUD I. 2013. Structure and vibrational spectroscopy of the fenbufen-β-cyclodextrin inclusion complex. Vibrat Spectr 69: 30-39.

BOUGHORBEL S, JARRAY F & EL-ANBARI M. 2017. Optimal classifier for imbalanced data using Matthews Correlation Coefficient metric. PLoS One 12(6): e0177678.

BURGOS AE & SINISTERRA RD. 2010. Preparación y caracterización de compuestos de asociación entre el acetato, propionato y butirato de rodio(II) con β-ciclodextrina. Rev Colomb Quím 39(3): 427-445.

CHANG CC & LIN CJ. 2011. LIBSVM: a library for support vector machines. *ACM TIST*, 2(3): 1-27. Software available at http://www.csie.ntu.edu.tw/~cjlin/libsvm. Accessed on 28 August 2018.

CLSI - CLINICAL & LABORATORY STANDARDS INSTITUTE. 2003. Performance standards for antimicrobial disk susceptibility testing. 8th ed., Wayne, Pa: Clinical and Laboratory Standards Institute, (Document M2-A8).

COWEN LE & LINDQUIST S. 2005. Hsp90 potentiates the rapid evolution of new traits: drug resistance in diverse fungi. Science 309(5744): 2185-2189.

COYLE B, KAVANAGH K, MCCLEAN M, DEVEREUX M & GERAGHTY M. 2003. Mode of anti-fungal activity of 1,10-phenanthroline and its Cu(II), Mn(II) and Ag(I) complexes. BioMetals 16(2): 321-329.

CULVER GM, MCCRAITH SM, CONSAUL SA, STANFORD DR & PHIZICKY EM. 1997. A 2'-Phosphotransferase Implicated in tRNA Splicing Is Essential in Saccharomyces cerevisiae. J Biol Chem 272(20): 13203-13210.

D'ARCY S & LUGER K. 2011. Understanding Histone Acetyltransferase Rtt109 Structure and Function: how many chaperones does it take? Curr Opin Struct Biol 21(6): 728-734.

DA ROSA CG, BORGES CD, ZAMBIAZI RC, NUNES MR, BENVENUTTI EV, DA LUZ SR, D'AVILA RF & RUTZ JK. 2013. Microencapsulation of gallic acid in chitosan, β-cyclodextrin and xanthan. Ind Crops Prod 46: 138-146.

DAS S & SUBUDDHI U. 2015. Studies on the complexation of diclofenac sodium with β-cyclodextrin: Influence of method of preparation. J MoleC Struct 1099: 482-489.

DE WINTER H & LOPES JCD. 2018. Reply to the comment made by Šicho, Voršilák and Svozil on 'The Power metric: a new statistically robust enrichment-type metric for virtual screening applications with early recovery capability'. J Cheminf 10(1): 14-15.

DEEGAN C, MCCANN M, DEVEREUX M, COYLE B & EGAN DA. 2007. *In vitro* cancer chemotherapeutic activity of 1,10-phenanthroline (phen), $[Ag_2(phen)_3(mal)]*2H_2O$, $[Cu(phen)_2(mal)]*2H_2O$ and $[Mn(phen)_2(mal)]*2H_2O$ ($malH_2$ = malonic acid) using human cancer cells. Cancer Lett. 247(2): 224-233.

DUARTE A, MARTINHO A, LUÍS A, FIGUEIRAS A, OLEASTRO M, DOMINGUES FC & SILVA F. 2015. Resveratrol encapsulation with methyl-β-cyclodextrin for antibacterial and antioxidant delivery applications. Food Sci Technol 63(2): 1254-1260.

DUCHÊNE D & BOCHOT A. 2016. Thirty years with cyclodextrins. Int J Pharmac 514(1): 58-72.

GARNERO C, CHATTAH AK & LONGHI M. 2014. Improving furosemide polymorphs properties through supramolecular complexes of β-cyclodextrin. J Pharmac Biomed Anal 95: 139-145.

GKANIATSOU E, BANTI CN, KOURKOUMELIS N, SKOULIKA S, MANOLI M, TASIOPOULOS AJ & HADJIKAKOU S. 2015. Novel mixed metal Ag(I)-Sb(III)-metallotherapeutics of the NSAIDs, aspirin and salicylic acid: Enhancement of their solubility and bioactivity by using the surfactant CTAB. J Inorg Biochem 150(284): 108-119.

HARDING HP, LACKEY JG, HSU HC, ZHANG Y, DENG J, XU RM, DAMHA MJ & RON D. 2008. An intact unfolded protein response in *Trpt1* knockout mice reveals phylogenic divergence in pathways for RNA ligation. RNA 14(2): 225-232.

HO B, JOYCE D & BHANDARI B. 2016. Novel solid encapsulation of ethylene gas using amorphous α-cyclodextrin and the release characteristics. J Agr Food Chem 64(17): 3318-3323.

KORYTKOWSKA-WAŁACH A, DUBRAWSKA B, SMIGA-MATUSZOWICZ M & BIEG T. 2017. Spectroscopic study on the inclusion complexes of β-cyclodextrin with selected metabolites of catecholamines. J Mol Struct 1127: 532-538.

LIMA PSS, LUCCHESEA AM, ARAÚJO-FILHO HG, MENEZES PP, ARAÚJO AAS, QUINTANS-JÚNIOR LJ & QUINTANS JSS. 2016. Inclusion of terpenes in cyclodextrins: Preparation, characterization and pharmacological approaches. Carboh Polym 151: 965-987.

LIU B, ZHOU H, ZHOU S & YUAN J. 2015. Macromolecules based on recognition between cyclodextrin and guest molecules: Synthesis, properties and functions. Eur Polym J 65: 63-81.

LOPES JCD, DOS SANTOS FM, MARTINS-JOSÉ A, AUGUSTYNS K & DE WINTER H. 2017. The power metric: a new statistically robust enrichment-type metric for virtual screening applications with early recovery capability. J Cheminf 98(1): 7.

LUCIO D, IRACHE JM, FONT M & MARTÍNEZ-OHÁRRIZ MC. 2017. Nanoaggregation of inclusion complexes of glibenclamide with cyclodextrins. Intern J Pharmac 519(1-2): 263-271.

MEINGUET C, MASEREEL B & WOUTERS J. 2015. Preparation and characterization of a new harmine-based antiproliferative compound in complex with cyclodextrin: Increasing solubility while maintaining biological activity. Eur J Pharmac Sci 77: 135-140.

MOHAN PRK, SREELAKSHMI G, MURALEEDHARAN CV & JOSEPH R. 2012. Water-soluble complexes of curcumin with cyclodextrins: Characterization by FT-Raman spectroscopy. Vibrat Spectr 62: 77-84.

MOYANO DF, MURCIA LE, PARRA DA, BURGOS AE & ARISTIZABAL FA. 2012. Evaluación de la actividad citotóxica y antimicrobiana del compuesto [Ag(phen)$_2$]salH. Rev Colomb Quím 41(1): 47-59.

MUJAHID M ET AL. 2016. Novel silver(I) complexes of coumarin oxyacetate ligands and their phenanthroline adducts: Biological activity, structural and spectroscopic characterisation. J Inorg Biochem 163: 53-67.

NAJLAOUIA F, PIGEONB P, ABDELKAFIA Z, LECLERCD S, DURANDE P, EL-AYEBA M, MARRAKCHIA N, RHOUMAF R, JAOUENB G & GIBAUD S. 2015. Phthalimido-ferrocidiphenol cyclodextrin complexes: Characterization and anticancer activity. Int J Pharmac 491(1-2): 323-334.

NAKANO M, FUJIWARA T & KOGA N. 2016. Thermal Decomposition of Silver Acetate: Physico-Geometrical Kinetic Features and Formation of Silver Nanoparticles. J Phys Chem C 120(16): 8841-8854.

NORDMANN P, NAAS T & POIREL L. 2011. Global spread of carbapenemase-producing Enterobacteriaceae. Emerg Infect Dis 17(10): 1791-1798.

OLOMBRADA M, LÁZARO-GORINES R, LÓPEZ-RODRÍGUEZ JC, MARTÍNEZ-DEL-POZO A, MERCEDES OÑADERRA M, MAESTRO-LÓPEZ M, LACADENA J, GAVILANES JG & GARCÍA-ORTEGA L. 2017. Fungal Ribotoxins: A Review of Potential Biotechnological Applications. Toxins (Basel) 9(2): 71.

PACE CN, HEINEMANN U, HAHN U & SAENGER W. 1991. Ribonuclease T1: Structure, Function, and Stability. Angew Chem 30(4): 343-360.

PALZKILL T. 2013. Metallo-β-lactamase structure and function. Ann N Y Acad Sci 1277: 91-104.

PRADINES B, GALLARD J, IORGA BI, GUEUTIN C, LOISEAU PM, PONCHEL G & BOUCHEMAL K. 2014. Investigation of the complexation of albendazole with cyclodextrins for the design of new antiparasitic formulations. Carboh Res 398: 50-55.

REEDY JL, FILLER SG & HEITMAN J. 2010. Elucidating the *Candida albicans* calcineurin signaling cascade controlling stress response and virulence. Fungal Genetic Biol 47(2): 107.

ROCHA MP, CAMPANA PRV, SCOARIS DO, ALMEIDA VL, LOPES JCD, SILVA AF, PIETERS L & SILVA CG. 2018. Biological activities of extracts from *Aspidosperma subincanum* Mart. and *in silico* prediction for inhibition of acetylcholinesterase. Phytother Res 32(10): 2021-2033.

ROSA JL, BOYARTCHUK VL, ZHU LJ & KAUFMAN PD. 2010. Histone acetyltransferase Rtt109 is required for *Candida albicans pathogenesis*. Proceed Nat Acad Sci USA 107(4): 1594-1599.

RUTHERFORD ST & BASSLER BL. 2012. Bacterial quorum sensing: its role in virulence and possibilities for its control. Cold Spring Harb Perspect Med 2(11): a012427.

SANTOS FM, DE WINTER H, AUGUSTYNS K & LOPES JCD. 2015. Use of extensive cross-validation and bootstrap application (ExCVBA) for molecular modeling of some pharmacokinetics properties. Poster presented at OPENTOX EURO 2015 - OpenTox InterAction Meeting - Innovation in predictive toxicology, Dublin, Ireland.

SHAHABADI N, MAGHSUDI M & AHMADIPOUR Z. 2014. Study on the interaction of silver(I) complex with bovine serum albumin by spectroscopic techniques. Spectrochim Acta Part A 92: 184-188.

SHEMETULSKIS NE, WEININGER D, BLANKLEY CJ, YANG JJ & HUMBLET C. 1996. Stigmata: an algorithm to determine structural commonalities in diverse datasets. J Chem Inf Comput Sci 36(4): 862-871.

SIEMANN S, BREWER D, CLARKE AJ, DMITRIENKO GI, LAJOIE G & VISWANATHA T. 2002. IMP-1 metallo-beta-lactamase: effect of chelators and assessment of metal requirement by electrospray mass spectrometry. Biochim Biophys Acta 1571(3): 190-200.

SINNIAH S, MOHAMAD S & MANAN N. 2015. Magnetite nanoparticles coated with β-cyclodextrin functionalized-ionic liquid: Synthesis and its preliminary investigation as a new sensing material. Appl Surf Sci 357(Part A): 543-550.

STEPNIAK A, BELICA-PACHA S, ROZALSKA S, DLUGONSKI J, URBANIAK P & PALECZ B. 2015. Study on a host-guest interaction of β-cyclodextrin with tebuconazole in water. J Molec Liq 211: 288-293.

TERAUCHI M, INADAA T, TONEGAWA A, TAMURA A, YAMAGUCHI S, HARADAA K & YUI N. 2016. Supramolecular inclusion complexation of simvastatin with methylated β-cyclodextrins for promoting osteogenic differentiation. Int J Biol Macromol 93(Part B): 1492-1498.

THORNTON L ET AL. 2016. Water-soluble and photo-stable silver(I) dicarboxylate complexes containing 1,10-phenanthroline ligands: Antimicrobial and anticancer chemotherapeutic potential, DNA interactions and antioxidant activity. J Inorg Biochem 159: 120-132.

VESTLAND T, JACOBSEN Ø, SANDE S, MYRSET A & KLAVENESS J. 2015. Compactible powders of omega-3 and β-cyclodextrin. Food Chem 185: 151-158.

VIGANOR L, HOWE O, MCCARRON P, MCCANN M & DEVEREUX M. 2017. The antibacterial activity of metal complexes containing 1,10-phenanthroline: potential as alternative therapeutics in the era of antibiotic. CurTop Med Chem 17(11): 1280-1302.

WANG L, LI S, TANG P, YAN J, XU K & LI H. 2015. Characterization and evaluation of synthetic riluzole with β-cyclodextrin and 2,6-di-O-methyl-β-cyclodextrin inclusion complexes. Carboh Polym 129: 9-16.

WANG Y, BRYANT SH, CHENG T, WANG J, GINDULYTE A, SHOEMAKER BA, THIESSEN PA, HE S & ZHANG J. 2017. PubChem BioAssay: 2017 update. Nucleic Acids Res 45(D1): D955-D963.

WU M, MAIER E, BENZ R & HANCOCK R. 1999. Mechanism of interaction of different class of cationic antimicrobial peptides with planar bilayers and with the cytoplasmic membrane of *Escherichia coli*. Biochemistry 38(22): 7265-7242.

WU Y, LI H, LU Z, LI H, RAO Z, GENG Y, SHI J & XU Z. 2014. Enhancement of steroid hydroxylation yield from dehydroepiandrosterone by cyclodextrin complexation technique. Steroids 84: 70-77.

YANG X, ZHAO Y, CHEN Y, LIAO X, GAO C, XIAO D, QIN Q, YI D & YANG B. 2013. Host-guest inclusion system of mangiferin with β-cyclodextrin and its derivatives. Mat Sci Enginer C 33(4): 2386-2391.

ZHANG J, WU D, JIANG K, ZHANG D, ZHENG X, WAN C, ZHU H, XIE X, JIN Y & LIN J. 2015. Preparation, spectroscopy and molecular modelling studies of the inclusion complex of cordycepin with cyclodextrins. Carboh Res 406: 55-64.

ZHU ZY, LUO Y, LIU Y, WANG XT, LIU F, GUO MZ, WANG Z, LIU AJ & ZHANG YM. 2016. Inclusion of chrysin in β-cyclodextrin and its biological activities. J Drug Deliv Sci Technol 31: 176-186.

ZOU F, LI Y, YU X, ZHANG J, HUANG X & QU Y. 2014. β-cyclodextrin improves the linearity of polyaniline synthesized enzymatically in AOT micellar solution. J Molec Catal B: Enz 104: 35-41.

SUPPLEMENTARY MATERIAL

Figures S1, S2, S3, S4, S5, S6, S7, S8.
Tables SI, SII.

How to cite

BRIÑEZ-ORTEGA E, ALMEIDA VL, LOPES JCD & BURGOS AE. 2020. Partial inclusion of bis(1,10-phenanthroline)silver(I) salicylate in β-cyclodextrin: Spectroscopic characterization, *in vitro* and *in silico* antimicrobial evaluation. An Acad Bras Cienc 92: e20181323. DOI 10.1590/0001-3765202020181323.

Manuscript received on December 12, 2018;
accepted for publication on May 3, 2019

EDWIN BRIÑEZ-ORTEGA[1,4]
https://orcid.org/0000-0002-6260-1018

VERA L. DE ALMEIDA[2]
https://orcid.org/0000-0002-4981-2216

JULIO C.D. LOPES[3]
https://orcid.org/0000-0002-5872-7611

ANA E. BURGOS[1]
https://orcid.org/0000-0001-6117-5312

[1]Universidad Nacional de Colombia, Departamento de Química, Grupo de Investigaciónen Química de Coordinación y Bioinorgánica, Facultad de Ciencias, Av. Cra 30, 45-03 Sede-Bogotá, Colombia

[2]Serviço de Fitoquímica e Prospecção Farmacêutica, Fundação Ezequiel Dias, Rua Conde Pereira Carneiro, 80, 30350-010 Belo Horizonte, MG, Brazil

[3]Grupo de Estudos em Quimioinformática/NEQUIM, Universidade Federal de Minas Gerais, Instituto de Ciências Exatas, Departamento de Química, Av. Antônio Carlos, 6627, 31270-901 Belo Horizonte, MG, Brazil

[4]Grupo de Investigación en Química Aplicada a la Sostenibilidad, Universidad ECCI, Departamento Ciencias Básicas, Cra 19, 49-20, Bogotá, Colombia

Correspondence to: **Ana E. Burgos**

E-mail: aeburgosc@unal.edu.co

Author contributions

The author Edwin Briñez-Ortega responsible for the synthesis, characterization, *in vitro* tests of the antimicrobial activity of the compounds, analysis and writing the draft of the manuscript. The authors Vera L. de Almeida and Julio C.D. Lopes analyzed *in silico* the antimicrobial activity of the compounds, preparation and writing. The author Ana E. Burgos conceptualization, preparation, writing and review of the latest version. These four authors were very committed to the development and conduct of the research.